International Journal of Hybrid Information Technology
Vol. 9, No.7 (2016), pp. 71-78
http://dx.doi.org/10.14257/ijhit.2016.9.7.08

3D Modeling Of GNSS Vector Tracking Receiver in Urban Area

Wang Jiang-An, Cai Gang, Lu Pan and Gao Tao

School of Information Engineering, Chang'an University, Xi'an 710064, China
jawang@chd.edu.cn

Abstract

3D maps may be treated as a new data source for urban navigation and used to improve positioning accuracy in urban canyons However, 3D digital maps are not available in most cities. This paper proposed a new approach to build a 3D model by using a GNSS VT receiver. The system architecture was described first, and then the method of 3D modeling by analyzing received data was presented. The premise for building the 3D model is signal classification. Analysis of data collected by the VT receiver was described in detail. Using a GNSS signal recorded in a dense urban environment showed the effectiveness of the proposed approach.

Keywords*: 3D modeling, vector tracking, GNSS, NLOS*

1. Introduction

Currently, the applications of a global navigation satellite system (GNSS) are rapidly gaining popularity. With the planned GPS modernization programs of the U.S., GLONASS of Russia, GALILEO of Europe, and the launch of quasi-zenith satellites by Japan, an improvement in the availability of satellite positioning is anticipated. Indeed, 30 GPS satellites and 17 GLONASS satellites have become available in February 2010, and they are expected to increase the application of in-car navigation system. However, the poor performance of GNSS receivers in urban canyons is a well-known problem in terms of accuracy and solution availability [1, 2]. The receiver delivers a position that can be biased by an error of more than 100 m [3–5], which limits the use of many applications. A typical problem in urban areas is multipath and non-line-of-sight (NLOS) effect. Multipath propagation occurs when GNSS signals bounce off buildings and reach the receiver's antenna via different paths with a traveling time longer than that of the line-of-sight (LOS) path. Multipath signals can be strong and have small relative delays, which make them difficult to distinguish from the desired path signal.

Various hardware-based correlators that are robust to the multipath effect have been developed [6–11], such as multipath estimating delay-locked loop. Referencing building geometry data and satellite positions has been suggested as a way to avoid the use of NLOS satellites or weighting down [12, 13]. GNSS can show improved positioning accuracy in conjunction with other sensors such as Wi-Fi and/or dead reckoning using inertial sensors, magnetic compass, and barometric altimeter [14, 15].

A new approach has recently been proposed to improve cross-street accuracy using GNSS assisted by knowledge derived from 3D building models close to the user of navigation devices [16]. 3D maps may be treated as a new data source for urban navigation and used to improve positioning accuracy in urban canyons [17, 18]. Peyret et al. [19] used digital maps to detect hidden satellites. Iwase et al. [20] used an altitude map to estimate the pseudorange error and utilized the error to weight satellite signals. A 3D digital map-assisted GNSS receiver can obtain good results in urban canyons. However, a 3D digital map is not available in most cities.

ISSN: 1738-9968 IJHIT

This study aims to achieve 3D building models beside a road from a GNSS vector tracking receiver. Most land vehicles pass through the same area of a road many times every day. Therefore, the recorded data can be stored and analyzed to generate a 3D map near the road.

2. 3D Surveying Techniques and 3D Modeling

2.1. System Architecture

The 3D modeling system architecture is shown in Figure 1. An antenna collects the GNSS signal and relays it to the designed GNSS vector tracking receiver, which is described in detail in Section 3. Vector tracking (VT) code discriminator output is used to separate the NLOS signal from all received signals, and time output is synchronously stored as timestamp. Ephemeris storage is the necessary condition to find all blocked signals (BS). Through data analysis and processing, signals are classified as LOS and BS/NLOS, and the azimuth and altitude angle of satellites can be obtained. The 3D model of buildings on both sides of a road cannot be created by using only the classified GNSS signals. Therefore, some constraints of 3D modeling need to be established, which are based on a real field.

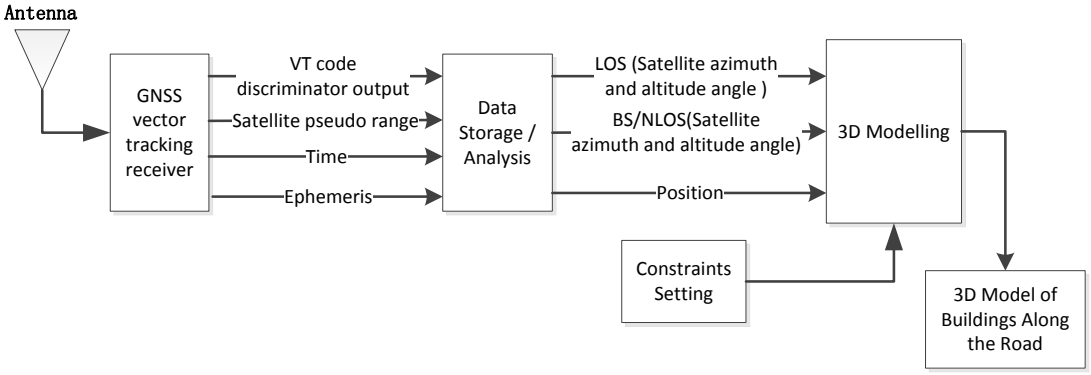

Figure 1. Architecture of 3D Building Modeling System.

2.2. Constraint Setting

Constraints are needed to combine with classified GNSS signal for the process of 3D modeling, and an accurate 3D model can be created with detailed constraints. To observe buildings on both sides of major roads in a city, some common rules are given as follows:

1. The width of the road is almost constant.
2. Most of the buildings can be equivalent as a cuboid.
3. The buildings on the both sides of the road are assumed to have the same width.

A 3D model is established in this paper is to assist the GNSS receiver in obtaining more accurate positioning results in urban canyons. Therefore, building a 3D model that is similar to the actual object is unnecessary. The above rules can be used to generate constraints. The width of the road W_0 (including the width of the sidewalk on both sides of the road) can be easily obtained by a digital 2D map. According to rough statistics result, the width of buildings can be unified as W_1.

2.3. 3D modeling Method

While the land vehicle is moving, all necessary data are stored in our system. The satellite azimuth and altitude angle (j, q) of LOS and BS/NLOS for each positioning result was obtained through data storage and analysis. The NLOS signals can be detected only dozens of

seconds later. Therefore, each positioning result is postprocessed to remove the effect of NLOS signal. The azimuth angle of a land vehicle running in a certain direction along a road is a . The GNSS signal is not blocked in the front and the back directions of a road. Thus, the satellite signal will not be used for 3D modeling if its azimuth angle

$$|j - a| \pounds 45^{o} \text{ or } |j + 180^{o} - a| \pounds 45^{o} \quad (1)$$

Also, the satellite altitude angle should satisfy the inequality

$$q \, ^{3} \, 15^{o} \quad (2)$$

If the satellite does not meet the above condition, its information will not be stored.

The width of the road W_0 , the uniform width of building W_1 and the antenna height H_0 are set as constant values. Thus, only the height and length of the building H_1 needs to be determined. The height and length of the building should meet the requirements for directly receiving the LOS signal and blocking the BS/NLOS signal. If the height is less than 3 m, the building is assumed to be non-existent on the ground in the 3D modeling process. Therefore, a 3D model of buildings on both sides of the road in urban areas can be constructed. The process of acquiring the information of LOS, NLOS, and BS separately will be discussed in the next section.

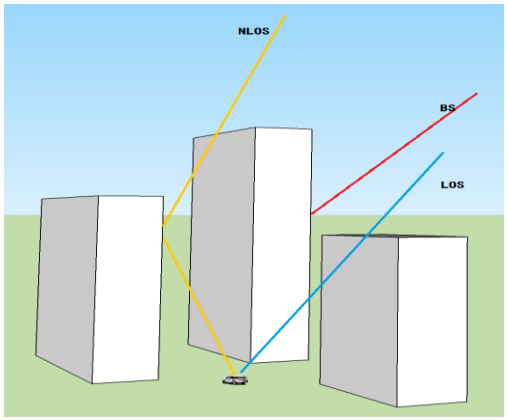

Figure 2. Schematic Diagram of 3D Modeling.

3. Signal Classification

VT [21, 22] is used in our receiver, and VT code discriminator output was stored by the system. Simultaneously, satellite pseudorange, ephemeris, and time information are also stored. With postprocessing, the effects of multipath interference and NLOS reception can be mitigated, and a better positioning result can be obtained. Moreover, long-path-delay NLOS signal can be separated from the received signals.

For each satellite signal receiving channel, the incoming signal is correlated with six locally generated replica signals: in-phase (I) and quadrant-phase (Q) early (E), prompt (P), and late (L). The incoming signal is correlated with a linear combination of reference signals subject to different delays, and the code discriminator is

$$d_{strobe} = \frac{ID \times IP + QD \times QP}{IP^2 + QP^2} \quad (3)$$

where ID and QD are the in-phase and quadrature components of the strobe correlators, respectively, and IP and QP are the in-phase and quadrature components, respectively, of prompt code correlators.

An EKF is used to correct the position and velocity solution using the code discriminator outputs and Doppler shift estimates. The measurements that are input to the EKF are delta

pseudorange Δr^j, and pseudorange rate $\dot{r}^j$. The delta pseudorange is the difference between the true and predicted pseudorange. They are calculated in the pre-filter by using

$$\Delta r^j = d^j \cdot \frac{c}{f_0} \tag{4}$$

$$\dot{r}^j = f_{Doppler}^j \cdot \frac{c}{f_{L1}} \tag{5}$$

where d is the code discriminator output in chips, $f_{Doppler}$ is the Doppler frequency in Hz, c is the speed of light, f_0 is the code chipping rate, and f_{L1} is the L1 band carrier frequency. The corrected receiver velocity and clock drift solution are used to update the position and clock offset every 20 ms, from which each of the pseudoranges are predicted using

$$\hat{r}_{R,k}^j = \sqrt{\left(\hat{r}_s^j - \hat{r}_a^-\right)^T \left(\hat{r}_s^j - \hat{r}_a^-\right)} + d\hat{r}_{SV,C}^j + d\hat{r}_T^j + d\hat{r}_I^j - \hat{b}_k \tag{6}$$

where $\hat{r}_s^j$ is the position of the satellite denoted by index j, determined from the broadcast ephemeris; $\hat{r}_a^-$ is the predicted receiver position; $d\hat{r}_{SV,C}^j$ is the satellite clock correction; $d\hat{r}_T^j$ and $d\hat{r}_I^j$ are the tropospheric and ionospheric error estimates, respectively; and $\hat{b}_k$ is the estimated receiver clock bias. The predicted pseudoranges are then used to generate the code NCO commands using

$$\hat{f}_{co,NCO\,j,\ k+1} = f_0 \left[1 - \frac{\left(\hat{r}_{R,k+1}^j - \hat{r}_{R,k}^j\right)}{ct_a}\right] \tag{7}$$

where t_a is the interval between epochs k and $k+1$. The state vector $\mathbf{x}$ thus comprises the following states:

$$\mathbf{x}^T = [\Delta p_{xk}\ \Delta p_{yk}\ \Delta p_{zk}\ \Delta v_{xk}\ \Delta v_{yk}\ \Delta v_{zk}\ \Delta b_k\ \Delta d_{clk,k}] \tag{8}$$

where Δp_k, Δv_k, Δb, and Δd_{clk} are the position, velocity, receiver clock bias, and drift, respectively. The transition matrix is

$$\mathbf{\Phi} = \begin{bmatrix} \mathbf{I}_{3\times 3} & \tau_s \mathbf{I}_{3\times 3} & \mathbf{0}_{3\times 2} \\ \mathbf{0}_{3\times 3} & \mathbf{I}_{3\times 3} & \mathbf{0}_{3\times 2} \\ \mathbf{0}_{2\times 3} & \mathbf{0}_{2\times 3} & \mathbf{\Phi}_{\mathbf{clk}} \end{bmatrix}_{8\times 8}, \quad \mathbf{\Phi}_{clk} = \begin{bmatrix} 1 & t_s \\ 0 & 1 \end{bmatrix} \tag{9}$$

where t_s is the EKF update interval. The system (or process) noise covariance matrix may be divided into user dynamic noise and receiver clock noise as follows:

$$\mathbf{Q} = \begin{bmatrix} \mathbf{B}_{\mathbf{dynamic}} & \mathbf{0}_{6\times 2} \\ \mathbf{0}_{2\times 6} & \mathbf{B}_{\mathbf{clock}} \end{bmatrix} \tag{10}$$

where

$$\mathbf{B}_{\mathbf{dynamic}} = \begin{bmatrix} \frac{t_s^3}{3}\times\mathbf{I}_{3\times 3} & \frac{t_s^2}{2}\times\mathbf{I}_{3\times 3} \\ \frac{t_s^2}{2}\times\mathbf{I}_{3\times 3} & t_s\times\mathbf{I}_{3\times 3} \end{bmatrix} \times S_v \tag{11}$$

$$\mathbf{B}_{\mathbf{clock}} = \begin{bmatrix} S_{cf} t_s + \frac{S_{cf} t_s^3}{3} & \frac{S_{cf} t_s^3}{2} \\ \frac{S_{cf} t_s^2}{2} & S_{cf} t_s \end{bmatrix} \quad \begin{matrix} S_{cf} = c^2 \times \frac{h_0}{2} \\ S_{cf} = c^2 \times 2p^2 \times h_{-2} \end{matrix} \tag{12}$$

where S_v is the user velocity noise power spectral density (PSD), S_{cf} is the oscillator phase noise PSD, and S_{cf} is the oscillator frequency noise PSD. h_0 and h_{-2} are clock model coefficients. The measurement vector is

$$d_{Z_k^-} = \begin{bmatrix} \Delta r_k^1 & \Delta r_k^2 & \mathrm{L} & \Delta r_k^m & \Delta \dot{r}_k^1 & \Delta \dot{r}_k^2 & \mathrm{L} & \Delta \dot{r}_k^m \end{bmatrix}^T \tag{13}$$

where Δr_k^j and $\Delta \dot{r}_k^j$ are the delta pseudorange and delta pseudorange rate, respectively, for satellite j at epoch k. The measurement matrix, which comprises the partial derivatives of the measurements with respect to the states, is

$$\mathbf{H} = \begin{bmatrix} \mathbf{U} & 0_{m \times 3} & 1_{m \times 1} & 0_{m \times 1} \\ 0_{m \times 3} & \mathbf{U} & 0_{m \times 1} & 1_{m \times 1} \end{bmatrix} \tag{14}$$

$$\mathbf{U} = \begin{bmatrix} -u_x^1 & -u_y^1 & -u_z^1 \\ -u_x^2 & -u_y^2 & -u_z^2 \\ \mathrm{M} & \mathrm{M} & \mathrm{M} \\ -u_x^m & -u_y^m & -u_z^m \end{bmatrix} \tag{15}$$

where m is the number of satellites, and u is the vector from the receiver to the satellite.

The VT code discriminator output has a large negative value during most of the period of NLOS reception. Furthermore, the highest correlation value is found in the late channel. Both phenomena provide an indication of potential NLOS reception. If the code discriminator output exceeds a pre-determined value, an abnormal output is assumed and a counter is incremented by one. If the counter value exceeds the pre-determined threshold N in a time window T_{window}, NLOS signal is detected; otherwise, the counter is reset to zero.

The GNSS receiver is unable to collect BS signals, and the VT receiver can eliminate multipath itself. Thus, only LOS and NLOS signals can be received. Therefore, based on the fact that the NLOS signals have been detected, the rest of the received signals are LOS.

The satellite signal that should be received can be predicted according to the ephemeris ($q \geq 15^o$), but LOS and NLOS are the signals that can actually be received. As a result, BS is the signal that should be received, but is not received by the GNSS receiver.

4. Experiments

The equipment used in the experiments is shown in Figure 3, where the VT receiver was designed with the implementation of DSP and FPGA devices.

Figure 3. Equipment Used in the Experiments.

We selected a stretch of Changa'an Road in Xi'an City as the experiment field, which is an open area surrounded by buildings. Both multipath interference and NLOS reception were present along many parts of the route. The latitude and longitude of the starting point is ($34^{o}13¢51.078¢¢$, $108^{o}56¢31.137¢¢$), and the end point is ($34^{o}13¢38.858¢¢$, $108^{o}56¢31.095¢¢$). The average elevation of the field is about 451m. Figure 4 shows the real driving route of the land vehicle on a satellite map. Without blockage, 12 GNSS satellite signals can be received (GPS+Glonass).

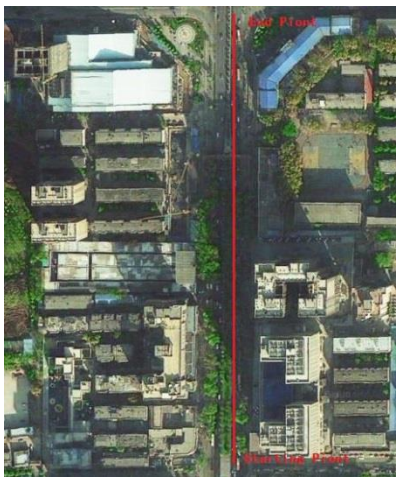

Figure 4. Real Driving Route.

The width of the road W_0 and the width of buildings W_1 are set to a constant value as constraints. Thus, only the building length and height need to be determined through data analysis. If data in this specific stretch of the road are collected and analyzed only once, then the built 3D model is shown in Figure 3(a). Within a short period of time for moving from the start point to the end point, the satellite azimuth and altitude angle $(j\ ,q)$ change minimally. Therefore, not enough signals are available to build an accurate model. However, an accurate 3D model was built when data were collected 10 times with long time intervals. The 3D model is shown in Figure 3(b).

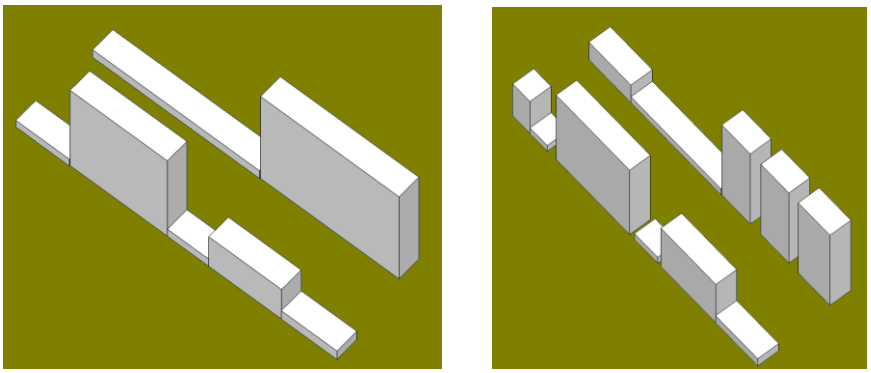

(a) 1 data collection (b) 10 data collection

Figure 5. 3D Model of Buildings on Both Sides of the Road.

5. Conclusion

A new approach to build a 3D model of buildings in an urban area based on GNSS VT receiver was proposed and implemented. Through analysis of data collected from a VT receiver, LOS/NLOS/BS can be obtained separately. With the preset constraint, a 3D model can be built with satellite azimuth and altitude angle of LOS/NLOS/BS. The effectiveness of the proposed approach was proved by using a GNSS signal recorded in a dense urban environment. The accuracy of the model could be improved through experiments with data collected multiple times with long time intervals.

Acknowledgments

The financial support of National Natural Science Foundation of China (61302150, 51408045) is acknowledged.

References

[1] Z. Jiang, G. Proves, W. Y. Ocheing, S. Feng, C. D. Milner and P. G. Mattos, "Multi-Constellation GNSS Multipath Mitigation Using Consistency Checking", ION GNSS 2011, Oregon Convention Center, Portland, Oregon, **(2011)**.
[2] P. D. Groves, "Shadow Matching: A New GNSS Positioning Technique for Urban Canyons", The Journal of Navigation, **(2011)**.
[3] E. Kaplan, "Understanding GPS: Principles and Application", 2nd Edition, Artech House, Norwood, MA, **(2006)**.
[4] O. Mezentsev, Y. Lu, G. Lachapelle and R. Klukas, "Vehicular navigation in urban canyons using a high sensitivity GPS receiver augmented with a low cost rate gyro", In Institute of Navigation GPS Conference,vol. 15, **(2002)**, pp. 263-369.
[5] J.H. Wang and Y. Gao, "High-sensitivity GPS data classification based on signal degradation conditions", Vehicular Technology, IEEE Transactions on, vol. 56, no. 2, **(2007)**, pp. 566-574.
[6] L. Garin and J.M. Rousseau, "Enhanced strobe correlator multipath rejection for code & carrier", In Proceedings of the 10th International Technical Meeting of the Satellite Division of The Institute of Navigation (ION GPS 1997), **(1997)**, pp. 559-568.
[7] A.J. Van Dierendonck, P. Fenton and T. Ford, "Theory and performance of narrow correlator spacing in a GPS receiver. Navigation", vol. 39, no. 3, **(1992)**, pp. 265-283.
[8] B. Townsend and P. Fenton, "A practical approach to the reduction of pseudorange multi path errors in an Ll GPS receiver", In Proceedings of the 7th International Technical Meeting of the Satellite Division of the Institute of Navigation, Salt Lake City, UT, USA, **(1994)**.
[9] M.S. Braasch, "Performance comparison of multipath mitigating receiver architectures", In Aerospace Conference, 2001, IEEE Proceedings., vol. 3, **(2001)**, pp. 1309-1315.
[10] B.R. Townsend, P.C. Fenton, KJ Van Dierendonck and D. J.R.Van Nee, "Performance evaluation of the multipath estimating delay lock loop", NAVIGATION-LOS ANGELES AND WASHINGTON, vol. 42, **(1995)**, pp. 503-514.
[11] P.C. Fenton and J. Jones, "The Theory and Performance of NovAtel Inc. ' s Vision Correlator", ION GNSS, **(2005)**.

[12] E. Costa, "Simulation of the effects of different urban environments on GPS performance using digital elevation models and building databases", Intelligent Transportation Systems, IEEE Transactions on, vol. 12, no. 3, **(2011)**, pp. 819–829.
[13] J. .Marais, M. Berbineau and M. Heddebaut, "Land mobile GNSS availability and multipath evaluation tool. Vehicular Technology", IEEE Transactions on, vol. 54, no. 5, **(2005)**, pp. 1697–1704.
[14] P. D. Groves, "Principles of GNSS, Inertial and Multisensor Integrated Navigation Systems", First Edition, Boston, London, Artech House, **(2008)**.
[15] J. A. Farrell, "Aided navigation: GPS with high rate sensors", McGraw-Hill Professional, **(2008)**.
[16] P. D. Groves, "Shadow Matching: A New GNSS Positioning Technique for Urban Canyons", The Journal of Navigation, **(2011)**.
[17] H. I. Kim, K. D. Park and H. S. Lee, "Development and Validation of an Integrated GNSS Simulator Using 3-D Spatial Information", Journal of the Korean Society of Surveying Geodesy Photogrammetry and Cartography, vol. 27, **(2009)**, pp. 659–667.
[18] L. Wang, P. Groves and M. Ziebart, "Gnss Shadow Matching Using A 3-D Model of London", Proceedings of the European Navigation Conference, Grange Tower Bridge, London, **(2011)**.
[19] F. Peyret, D. Bétaille, M. Ortiz, S. Miquel and L. Fontenay, "How to improve GNSS positioning Quality of Service for demanding ITS in city environments by using 3D digital maps", 19th ITS World Congress, Vienna, **(2012)**.
[20] T. Iwase, N. Suzuki and Y. Watanabe, "Estimation and exclusion of multipath range error for robust positioning", GPS solutions, vol. 17, no. 1, **(2013)**, pp. 53–62.
[21] L.T. Hsu, "Integration of vector tracking loop and multipath mitigation technique and its assessment", In: Proceedings of ION GNSS 2013, Institute of Navigation Nashville, Tennessee, **(2013)**, pp. 3263–3278.
[22] M. Lashley and D.M.Bevly, "Comparison in the performance of the vector delay/frequency lock loop and equivalent scalar tracking loops in dense foliage and Urban Canyon", In: Proceedings of ION GNSS 2011, Institute of Navigation Portland, Oregon, September, **(2011)**, pp 1786–1803.

Authors

Wang Jiang-An, he received the B.E. and the M.E. degrees from XiDian University, Xi'an, China, in 2003 and 2006 respectively, and the Ph.D. degree is received from XiDian University in 2010 in Electronic Science and Technology. From 2006 to 2010 he did multiple internships in HuaXun Microelectronic Corporation, Xi'an, working on Baseband Algorithm for GPS system. He joined the School of Information Engineering, Chang' an University, Xi'an, China in 2010 as a lecturer. His research interests include navigaiton and computer vision.

